Research Square

Preprints are preliminary reports that have not undergone peer review.
They should not be considered conclusive, used to inform clinical practice,
or referenced by the media as validated information.

miR-195-3p alleviates atherosclerosis by regulating VSMC functions through JNK2/NF-κB pathway

Pan Hou
General Hospital of Central Theater Command
Tongwei Lv
Second Medical Center, General Hospital of the Chinese People's Liberation Army
Qing Lu
General Hospital of Central Theater Command
Xianxian Zhao
Changhai Hospital, Naval Medical University
Shifang Ding
dingsfwh@163.com

General Hospital of Central Theater Command

Article

Keywords: miR-195-3p, vascular smooth muscle cells, JNK2, NF-κB, phenotypic switching, inflammation

Posted Date: November 1st, 2026

DOI: https://doi.org/10.21203/rs.3.rs-11102305/v1

License: This work is licensed under a Creative Commons Attribution 4.0 International License.
Read Full License

Additional Declarations: No competing interests reported.

Abstract

Background and Aim:

Atherosclerosis is a chronic inflammatory vascular disease and the primary pathological driver of life-threatening cardiovascular diseases. Vascular smooth muscle cells (VSMCs) contribute critically to vascular remodeling; their aberrant proliferation, migration, phenotypic switching and inflammatory activation promote atherosclerotic lesion development. miR-195-3p is a potential vasculo-protective microRNA, yet its exact functions and downstream mechanisms in VSMC-related atherosclerosis remain poorly defined. This study investigated the biological role of miR-195-3p in VSMCs and its molecular regulatory axis.

Methods and Results

miR-195-3p expression was measured in plasma from patients with coronary artery disease, atherosclerotic aortas from high-fat diet-fed ApoE$^{-/-}$ mice, and pathologically stimulated VSMCs. miR-195-3p was significantly downregulated under atherosclerotic conditions. Gain- and loss-of-function assays showed that miR-195-3p overexpression suppressed VSMC proliferation, migration and inflammation while preserving the contractile phenotype, whereas miR-195-3p inhibition induced pathological VSMC dysfunction. Transcriptomic, bioinformatic and dual-luciferase assays identified JNK2 as a direct target of miR-195-3p. Rescue experiments confirmed JNK2 mediates miR-195-3p's protective effects, and JNK2 aggravates VSMC dysfunction partly through activating the NF-κB inflammatory cascade. In ApoE$^{-/-}$ mice, AAV-mediated miR-195-3p overexpression reduced plaque burden, repressed JNK2/NF-κB signaling, restored VSMC homeostasis and mitigated vascular inflammation.

Conclusions

miR-195-3p maintains VSMC homeostasis and alleviates atherosclerosis by directly targeting JNK2 and inhibiting the NF-κB cascade. The miR-195-3p/JNK2/NF-κB axis enriches our understanding of atherosclerosis pathogenesis and offers candidate molecular targets for atherosclerotic cardiovascular disease therapy.

1. Introduction

Atherosclerosis is the primary pathological basis of life-threatening cardiovascular events including myocardial infarction, ischemic stroke and peripheral arterial disease, ranking as the leading cause of global mortality [1]. Vascular smooth muscle cells (VSMCs), the dominant cellular constituent of the arterial media, are central drivers of atherosclerotic lesion formation and progression. Under physiological conditions, mature VSMCs maintain a differentiated contractile phenotype to sustain

vascular wall tension and homeostasis. Upon stimulation by pathological triggers such as platelet-derived growth factor-BB (PDGF-BB), hypoxia or excess serum lipids, VSMCs undergo phenotypic switching toward a synthetic state, characterized by enhanced proliferation, migratory capacity and pro-inflammatory secretory activity. Synthetic VSMCs accumulate within the subendothelial space, secrete extracellular matrix and pro-inflammatory cytokines, ultimately accelerating plaque growth, lipid deposition and vascular remodeling [2]. Targeting the molecular pathways that restrain VSMC synthetic transformation represents a promising therapeutic strategy for atherosclerosis intervention.

MicroRNAs (miRNAs) are short endogenous non-coding RNAs that post-transcriptionally repress target gene expression via complementary binding to the 3'-untranslated region (3'-UTR) of mRNA transcripts [3]. Accumulating evidence has identified numerous miRNAs as critical modulators of VSMC phenotypic homeostasis and atherosclerotic progression. miR-195 family members have been reported to exert protective effects against vascular inflammation, endothelial injury and lipid metabolic disorders in prior vascular studies [4–6]. However, existing literature regarding miR-195-3p remains limited: although its broad atheroprotective potential has been acknowledged, its specific functional roles and molecular targets in VSMCs are largely uncharacterized, with no systematic research clarifying how miR-195-3p regulates VSMC proliferation, migration, phenotypic switching and inflammatory activation during atherogenesis.

c-Jun N-terminal kinase 2 (JNK2, encoded by MAPK9) is a stress-activated mitogen-activated protein kinase with well-documented pro-atherogenic functions across multiple vascular cell compartments. Multiple in vivo genetic studies have validated that global or hematopoietic-specific deletion of JNK2 markedly reduces atherosclerotic plaque burden in hyperlipidemic ApoE$^{-/-}$ and LDLR$^{-/-}$ mice, largely by restraining macrophage foam cell formation and lipid uptake [7, 8]. JNK2 deletion also alleviates hypercholesterolemia-triggered endothelial dysfunction and vascular oxidative stress, which are early initiating events of atherosclerotic vascular injury [9]. In VSMCs, pathological stimuli including growth factors and inflammatory cytokines can activate JNK signaling cascades, which are broadly implicated in driving VSMC proliferative and migratory activity, two core pathological behaviors that fuel neointimal thickening and plaque progression [10, 11]. Moreover, JNK2 also plays a pivotal role in inflammatory crosstalk; published mechanistic research has established functional crosstalk between JNK signaling and the NF-κB inflammatory axis, the master transcriptional pathway governing vascular inflammatory reaction [12]. JNK activation facilitates NF-κB p65 phosphorylation and nuclear translocation, which subsequently induce the transcription of pro-atherogenic cytokines such as IL-6, IL-8 and TNF-α; conversely, pan-JNK pharmacological blockade suppresses NF-κB-driven inflammatory responses in VSMCs [13, 14].

Herein, we delineate a novel molecular regulatory cascade: miR-195-3p directly targets JNK2 to restrain NF-κB signaling activation, thereby inhibiting VSMC synthetic transformation and inflammatory reaction to alleviate atherosclerotic lesion development. This work identifies a previously unrecognized miR-195-

3p/JNK2/NF-κB axis that maintains VSMC homeostasis and expands the regulatory network of atherosclerosis, providing potential molecular targets for anti-atherosclerotic therapy.

2. Material and methods

2.1 Cell Culture and treatment

Human primary aortic vascular smooth muscle cells (HA-VSMCs) used in this study were purchased from the American Type Culture Collection (ATCC, Cat No. PCS-100-012). The cells were cultured in smooth muscle cell medium (SMCM, Cat No. 1101) specifically designed for primary vascular smooth muscle cells, obtained from ScienCell (USA), supplemented with fetal bovine serum (FBS) at a final concentration of 2% and smooth muscle growth supplement (SMGS). 293T cells were maintained in Dulbecco's Modified Eagle Medium (DMEM, Cat No. C12430500BT) containing 10% FBS. To establish the disease model, HA-VSMCs were cultured in SMCM supplemented with 10% FBS or PDGF-BB at a final concentration of 20ng/ml. For hypoxic treatment, VSMCs were cultured in a hypoxic incubator maintained at 1% O_2, 5% CO_2, and balanced with nitrogen. Normoxic control cells were incubated under 37℃, 21% O_2 and 5% CO_2 conditions.

2.2 RNA isolation, reverse transcription, and quantitative real-time PCR

Total RNA was extracted using the AG RNAex Pro RNA Extraction Kit (TRIzol, Accurate Biotechnology, Cat No. AG21101) following the manufacturer's instructions. After quantification, RNA was aliquoted and stored at -80℃. Total RNA was subjected to quality validation (A260/A280 ratio ranging from 1.8 to 2.1) before reverse transcription. For mRNA, HiScript III RT SuperMix for qPCR (+ gDNA wiper; Vazyme, Cat No. R323-01) was used to synthesize cDNA. For miRNA, tailing was first performed using the miRNA Tailing and Reverse Transcription Kit (Accurate Biotechnology, Cat No. AG11716), followed by reverse transcription. Quantitative real-time polymerase chain reaction (qRT-PCR) was performed using SYBR® Green Real-time PCR Master Mix (TOYOBO, Cat No. QPK-101). The primer sequences for target genes are listed in Supplementary Table 1. GAPDH and U6 were employed as internal references for mRNA and miRNA, respectively. The relative expression levels of genes were calculated using the $2^{-\Delta\Delta Ct}$ method.

2.3 Oligonucleotide Transfection

RNA oligonucleotides including miR-195-3p mimic, miR-195-3p inhibitor, JNK2 siRNA and negative controls were purchased from GenePharma. Sequences of these oligonucleotides are listed in Supplementary Table 2. Transfection was performed using iMAX Transfection Reagent (Invitrogen, Cat No. 178150) according to the manufacturer's protocol. The culture medium was replaced 24 h after transfection. RNA and protein expression levels were detected at 24–72 h and 48–96 h post-transfection, respectively.

2.4 MicroRNA and RNA sequencing analysis

Transcriptome sequencing was performed in vascular smooth muscle cells (VSMCs) with miR-195-3p overexpression to obtain the differentially expressed gene profile. Differential expression analysis was conducted using the DESeq2 software package, with a screening threshold of $|\log_2 FoldChange| > 2$ and adjusted p-value < 0.05. KEGG pathway enrichment analysis (FDR < 0.05) was performed on differentially expressed genes to identify biological pathways potentially regulated by miR-195-3p. Candidate target genes were systematically selected by combining differentially expressed genes, KEGG enrichment results, and target gene predictions from the TargetScan and miRDB databases. The GSE100927 dataset was analyzed using GSEA software (version 4.2.3) to explore JNK2-related signaling pathways. Samples were divided into high- and low-expression groups based on the median expression level of JNK2. The analysis used the canonical pathway gene set (c2.cp.v2024.1.Hs.symbols.gmt) and GO functional annotation gene set (c5.go.v2024.1.Hs.symbols.gmt) from the MSigDB database. Significant enrichment was defined as a nominal p-value < 0.05 and false discovery rate (FDR) < 0.25.

2.5 VSMC proliferation analysis

Cell proliferation was detected using the 5-ethynyl-2'-deoxyuridine (EdU) incorporation assay. After pretreatment according to the manufacturer's instructions, the Click reaction solution was prepared, and cells were incubated in the dark for 30 min to complete fluorescent labeling. After washing, cells were stained with 1× Hoechst 33342 solution for 10 min to label nuclei. Following another wash, images were observed and captured under a fluorescence microscope.

2.6 VSMC migration analysis

Cell migration and repair capacity of vascular smooth muscle cells were evaluated by wound healing assay. Cells were treated for 24h as designed, and the medium was replaced with serum-free medium after scratching, followed by continuous incubation for 24 h. Images at 0 h were captured under a microscope as the baseline. Cells were returned to the incubator for another 24 h, and images of the same fields were recorded periodically. The wound width at 0 h and 24 h was analyzed using ImageJ, and the healing rate was calculated to assess cell repair.

Cell migration was further assessed using Transwell chambers (Corning, Cat No. 3422, 24-well, 8.0μm pore size). Cells were treated for 24h as designed. After digestion and resuspension, the treated cells were counted and seeded evenly into the upper chambers for each group, the lower chambers were filled with conditioned medium containing chemokines. After 24h culture, cells were stained with fixed with 4% paraformaldehyde (Beyotime, Cat No. P0099) and stained with crystal violet (Servicebio, Cat No. G1014), and three to five random fields were counted under a microscope. Quantitative analysis was performed using ImageJ.

2.7 Western blot

Western blot analysis was performed according to standard protocols. Cells or tissue samples were lysed in RIPA lysis buffer supplemented with protease inhibitors (New Cell & Molecular, Cat No. WB3100), and protein concentrations were determined using a BCA protein assay kit (Thermo Fisher, Cat

No. UE285903). A three-color pre-stained protein marker (Yase Medical Biotechnology, Cat No. WJ103) was used for molecular weight calibration. Protein samples were separated by SDS-PAGE (GenScript, Cat No. M0065680)(100 V for 15 min, followed by 120 V for 60 min) and transferred onto activated PVDF membranes (Millipore, Cat No. IPFL00010) using a wet transfer system (140 V, 120 min, 4℃).After blocking, membranes were incubated overnight at 4℃ with the following primary antibodies: TNF-α (Proteintech, Cat No. 17590-1-AP), IL-6 (Proteintech, Cat No. 21865-1-AP), IL-8 (Proteintech, Cat No. 27095-1-AP), SM22-α (Abcam, Cat No. ab213273), α-SMA (Bioss, Cat No. Bsm-33187M), JNK2 (Abways, Cat No. CY5623), STAT3 (Proteintech, Cat No.10253-2-AP), p65 (Proteintech, Cat No. 10745-1-AP), p-p65 (Proteintech, Cat No. 82335-1-RR) and the internal reference GAPDH (Abways, Cat No. AB0037). Horseradish peroxidase (HRP)-conjugated anti-rabbit IgG was obtained from Abways (Cat No. AB0101), and HRP-conjugated anti-mouse IgG was purchased from Abways (Cat No. AB0102). After washing, immunoreactive bands were visualized using ECL luminescent reagent (New Cell & Molecular, Cat No. P10300) and detected with a LAS4000 chemiluminescence imager (GE Healthcare). Band intensities were quantified using ImageJ, and the expression levels of target proteins were normalized to GAPDH.

2.8 Luciferase reporter assay

Dual-luciferase reporter assays were performed using the psiCHECK-2 vector. Sequences spanning 100 bp upstream and downstream of the predicted binding sites were synthesized and cloned into the vector by Sangon Biotech (Shanghai) Corp., Ltd. 293T cells were co-transfected with 50ng of the recombinant plasmid per well and miR-195-3p mimics or negative control mimics (final concentration 50nM) using Lipofectamine 2000 transfection reagent. Fluorescence intensity was measured with a microplate reader following the manufacturer's instructions for the dual-luciferase reporter assay kit (Yeasen, Cat No. 11402ES60). Relative luciferase activity was calculated to evaluate the expression changes of the target gene.

2.9 Generation of microRNA Adenovirus

For JNK2 overexpression, an adenovirus-mediated JNK2 overexpression and control adenovirus system was constructed by Obio Technology (Shanghai) Corp., Ltd. During the transduction procedure, the multiplicity of infection (MOI) was calculated according to the viral titer and the counted cell number.

2.10 Animal treatment

In this study, an atherosclerotic model was established in $ApoE^{-/-}$ mice by high-fat diet induction. Six-week-old male $ApoE^{-/-}$ mice were acclimated for 1 week with a normal chow diet, and then randomly divided into two groups: a high-fat diet model group (high-fat diet + control adeno-associated virus), and a miR-195-3p treatment group (high-fat diet + miR-195-3p adeno-associated virus). Mice received the corresponding virus via tail-vein injection during the induction period. High-fat diet induction lasted for 20 weeks, during which mice were housed in an SPF environment (temperature 22 ± 2℃, humidity 50 ± 10%, 12 h light-dark cycle). Sterile bedding was replaced weekly, and general condition were monitored. At the experimental endpoint, after 12 h of fasting, mice were anesthetized by intraperitoneal injection of pentobarbital sodium (50 mg/kg). The depth of anesthesia was verified by checking the absence of the

pedal withdrawal reflex. Subsequently, cardiac perfusion was performed, and aorta and heart tissues were collected. Humane euthanasia was achieved via exsanguination under deep anesthesia.

2.11 Immunohistochemistry and Immunofluorescence

Immunohistochemistry was performed on tissue samples. Aortas were fixed in 4% paraformaldehyde (Beyotime, Cat No. P0099), embedded in paraffin, and sectioned for detection using conventional immunohistochemical methods. Images were observed and captured under a light microscope. The primary antibody was p-p65 (Proteintech, Cat No. 82335-1-RR).

Immunofluorescence staining was performed on cell slides. After corresponding treatments, cells were fixed in 4% paraformaldehyde at room temperature, followed by standard procedures. After mounting, images were observed and captured under a fluorescence microscope. The primary antibody was α-SMA (Bioss, Cat No. bsm-33187M).

2.12 HE

Tissues were embedded in OCT compound (Beyotime, Cat No. C0171A-118ml) for frozen sectioning. After staining and mounting according to standard protocols, sections were observed under a light microscope, and quantitative analysis was performed using ImageJ.

2.13 Oil Red O

Tissues were embedded in OCT compound (Beyotime, Cat No. C0171A-118ml) and prepared for frozen sections. After staining and mounting following standard procedures, sections were observed under a microscope. Lipid deposition was indicated by orange-red areas, and quantitative analysis of plaque area was performed using ImageJ.

2.14 ELISA

The detection was performed using the SignalUp™ ELISA Ultrasensitive Detection Kit (Beyotime, Cat No. P0205S). After incubation according to the standard sandwich protocol, the fluorescence intensity was measured with a microplate reader, and the sample concentrations were calculated based on the standard curve.

2.15 Statistical Analysis

All measurement data are presented as the mean ± standard deviation (Mean ± SD). Each treatment group in the experimental design included at least 3 independent biological replicates. For statistical analysis: Comparisons between two groups were performed using the unpaired t test for data with equal variance or Welch's t test when variances were unequal. Comparisons among multiple groups were conducted using one-way analysis of variance (ANOVA) followed by Tukey's multiple comparison test. Differentially expressed miRNAs and mRNAs were screened using the DESeq2 algorithm. The significance level was set at $\alpha = 0.05$, and all hypothesis tests were two-sided. A value of $P < 0.05$ was

considered statistically significant. Data analysis was mainly performed using SPSS 26.0. Partial data calculations and all statistical graphs were generated using GraphPad Prism 8.0.

3. Results

3.1. miR-195-3p is downregulated in multiple models of VSMC proliferation and in the plasma of patients with CAD

Vascular smooth muscle cells (VSMCs) constitute a pivotal cellular contributor to atherosclerotic progression. Our study has long focused on deciphering the molecular mechanisms underlying VSMC-mediated atherosclerotic lesions. During preliminary investigation, we serendipitously observed that exogenous miR-195-3p overexpression triggered a prominent morphological phenotypic transition in VSMCs: cells shifted from an elongated, sharp spindle shape to a broad, plump flattened morphology (Fig. 1a). To interpret this intriguing phenomenon, we conducted a systematic literature review and identified that miR-195-3p exerts well-documented atheroprotective effects, yet its specific biological roles in VSMCs remain scarcely characterized [4]. We next quantified miR-195-3p expression across multiple clinically and experimentally relevant models. miR-195-3p levels were markedly reduced in plasma samples from patients diagnosed with coronary artery disease (CAD), as well as in aortic tissues harvested from high-fat diet-fed ApoE$^{-/-}$ mice (Fig. 1b, 1c). Consistently, diminished miR-195-3p abundance was detected in established VSMC proliferative models stimulated by hypoxia, PDGF-BB or FBS, and also in exosomes isolated from the culture supernatant of PDGF-BB treated VSMCs (Fig. 1d–1g).

Collectively, these data reveal that miR-195-3p is consistently downregulated in both clinical atherosclerotic specimens and animal atherosclerotic models, and its intracellular abundance in VSMCs exhibits a significant negative correlation with VSMC proliferative activity.

3.2 miR-195-3p regulates VSMC proliferation, migration, phenotypic switching and inflammatory response

Proliferation, migration and phenotypic switching of VSMCs are core pathological events driving atherosclerotic lesion initiation and progression. To dissect the biological function of miR-195-3p in VSMCs, we first validated the transfection efficiency of miR-195-3p mimic and inhibitor via qRT-PCR (Figure S1a, S1b), then performed a panel of cellular functional assays.

The 5-ethynyl-2'-deoxyuridine (EdU) proliferation assay revealed that miR-195-3p mimic significantly reduced VSMC proliferative capacity, whereas transfection with the miR-195-3p inhibitor notably promoted VSMC proliferation (Fig. 2a, 2c). Both wound healing and Transwell migration assays demonstrated that miR-195-3p mimic impaired VSMC migration, while its inhibitor significantly enhanced VSMC migration within 24 hours of incubation (Fig. 2b, 2d, 2e, 2f).

To clarify the morphological alterations of VSMCs induced by miR-195-3p mimic transfection, we detected the expression levels of smooth muscle α-actin (SMA) and smooth muscle 22α (SM22α), specific markers of the VSMC contractile phenotype. Consistent with our hypothesis, VSMCs transfected with miR-195-3p mimic exhibited significantly upregulated expression of SMA and SM22α, both at the mRNA and protein levels, while miR-195-3p inhibitor transfection led to significant downregulation of these two markers (Fig. 2g, 2h, 2j, 2k).

Atherosclerosis is widely recognized as a chronic inflammatory vascular disorder. The expression levels of inflammatory cytokines closely associated with atherosclerosis, including interleukin-6 (IL-6), interleukin-8 (IL-8), and tumor necrosis factor-α (TNF-α) [15]. Western blot analysis showed that miR-195-3p mimic transfection significantly downregulated the expression of these inflammatory cytokines, whereas miR-195-3p inhibitor significantly upregulated their expression (Fig. 2i, 2l).

Collectively, these findings demonstrate that miR-195-3p inhibits VSMC proliferation and migration, preserves its contractile phenotype, and suppresses its inflammatory activation.

3.3 miR-195-3p exerts its effects by targeting the 3'-untranslated region (3'-UTR) of JNK2

To elucidate the molecular mechanism underlying miR-195-3p-mediated regulation in VSMCs, we performed high-throughput transcriptome sequencing on VSMCs with stable miR-195-3p overexpression to screen candidate target genes. Using a threshold of $|\log_2 FC| \geq 2$, P-value < 0.05, FDR < 0.05. We identified 414 significantly upregulated and 763 markedly downregulated genes (Fig. 3a). Based on the well-established canonical miRNA regulatory paradigm—miRNAs typically bind the 3'-UTR of target mRNAs to trigger translational repression or mRNA degradation, we prioritized the downregulated gene set for KEGG pathway enrichment analysis and genes with the highest frequency of participation in enriched pathways were further extracted to obtain the core top gene set. (Fig. 3b,3c). Next, two authoritative online miRNA target prediction databases, TargetScan (https://www.targetscan.org) and miRDB (https://mirdb.org), were employed to predict miR-195-3p targets. Intersection analysis of database-predicted targets and KEGG enrichment top genes yielded three candidate genes: JNK2 (also known as MAPK9), RPS6KA5(Mitogen- and stress-activated protein kinase 1) and ZFP36 (Zinc finger protein 36) (Fig. 3d). Subsequent low-throughput qPCR validation confirmed more stable and consistent downregulation of JNK2 upon miR-195-3p overexpression (Fig. 3e). In addition, accumulated published evidence confirms JNK2 drives atherosclerotic progression via multiple vascular pathological pathways, making it the primary candidate for further functional validation.

Western blot analysis verified that JNK2 protein abundance was significantly reduced upon miR-195-3p overexpression (Fig. 3f). We then constructed a psi-CHECK2 vector containing wild-type or mutant JNK2 3'-UTR for dual-luciferase reporter assays. Co-transfection of miR-195-3p mimic markedly attenuated luciferase activity of the wild-type JNK2 3'-UTR reporter, with no significant change detected in the mutant group, which validated direct physical binding between miR-195-3p and the 3'-UTR of JNK2 (Fig. 3g).

3.4 JNK2 acts as the essential downstream mediator of miR-195-3p in VSMCs

As a core MAPK family member closely implicated in atherogenesis, JNK2 was confirmed as a direct target of miR-195-3p in the preceding experiments. We therefore conducted a series of rescue functional assays to characterize the independent biological function of JNK2 and determine whether it serves as the causal effector mediating miR-195-3p-induced VSMC phenotypic changes. qRT-PCR and Western blot validated satisfactory transfection efficiency of JNK2 siRNA and JNK2-overexpressing adenovirus (Figure S1c–S1f).

EdU proliferation assays showed that endogenous JNK2 silencing significantly suppressed VSMC proliferation, whereas adenovirus-mediated JNK2 overexpression robustly accelerated cell proliferation. Notably, co-transfection with miR-195-3p mimic effectively reversed the pro-proliferative phenotype triggered by excess JNK2 expression (Fig. 4a, 4c). Parallel trends were observed in wound healing and Transwell migration assays: JNK2 knockdown inhibited both horizontal and vertical migration, while JNK2 overexpression promoted migratory capacity; exogenous miR-195-3p overexpression could fully abrogate JNK2-driven migratory enhancement (Fig. 4b, 4d, 4e). At mRNA and protein levels, JNK2 silencing upregulated contractile markers SMA and SM22α, whereas JNK2 overexpression repressed their expression; miR-195-3p co-transfection counteracted JNK2-mediated phenotypic remodeling (Fig. 4f). In addition, we treated VSMCs with the selective JNK inhibitor SP600125 to block endogenous JNK signaling activation [16, 17]. Pharmacological blockade of JNK signaling abrogated the ability of miR-195-3p to elevate protein levels of SMA and SM22α (Figure S1g).

A similar trend was also observed in inflammatory responses. Western blot analysis revealed that JNK2 knockdown significantly reduced the transcription of inflammation cytokine IL-6, IL-8 and TNF-α, while JNK2 overexpression induced robust cytokine upregulation. Co-overexpression of miR-195-3p completely reversed the pro-inflammatory effect driven by elevated JNK2 (Fig. 4g).

Collectively, these data demonstrate that JNK2 elicits biological functions opposite to miR-195-3p in VSMCs, and JNK2 is the essential downstream effector mediating all core biological actions of miR-195-3p, including proliferation, migration, phenotypic switching and inflammatory regulation.

3.5 JNK2 mediates VSMC dysfunction by activating the NF-κB signaling pathway

To dissect the downstream functional cascades through which JNK2 mediates VSMC pathological remodeling, we performed gene set enrichment analysis (GSEA) on the public dataset GSE100927, stratifying samples into JNK2-high and JNK2-low subgroups. GSEA across KEGG, REACTOME and WikiPathways gene sets identified prominent enrichment of immune-inflammatory pathways (all NES > 2, $P < 0.05$), including TLR signaling, NOD-like receptor signaling, neutrophil degranulation and lysosomal pathways (Fig. 5a).

Consistent with these observations, GO biological process (GOBP) enrichment further revealed top functional terms centered on leukocyte/lymphocyte-mediated immunity, positive regulation of IL-6 biosynthesis and adaptive immune responses (all NES > 2, P < 0.05). Corresponding GO cellular component (GOCC) enrichments included tertiary granules (key organelles for neutrophil degranulation) and contractile muscle fibers, indicative of disrupted VSMC structural homeostasis (Fig. 5b). Critically, all enriched inflammation-related pathways converge on NF-κB signaling; separate GSEA of canonical, non-canonical and positive regulatory NF-κB gene sets confirmed robust NF-κB pathway activation in JNK2-high samples (Fig. 5c).

We next performed Western blot to determine whether JNK2 drives NF-κB pathway activation. JNK2 silencing markedly reduced phosphorylation of NF-κB core subunit p65 (p-p65) and downstream inflammatory transcription factor STAT3, while JNK2 overexpression strongly elevated p-p65 and STAT3 abundance. Importantly, co-transfection with miR-195-3p mimic effectively reversed JNK2-induced NF-κB hyperactivation (Fig. 5d). These experimental results recapitulate our bioinformatic predictions, confirming JNK2 as a potent positive regulator of NF-κB signaling.

Diprovocim is a selective NF-κB agonist. To dissect whether NF-κB signaling mediates JNK2-dependent VSMC phenotypic remodeling, we performed rescue functional assays with Diprovocim. Pharmacological activation of NF-κB significantly accelerated VSMC proliferation, enhanced both horizontal and vertical migratory capacity, and suppressed the expression of contractile markers SMA and SM22α. As expected, concurrent overexpression of miR-195-3p reversed all pro-atherogenic phenotypes induced by NF-κB agonist stimulation (Figure S2a–S2f).

Collectively, these results establish a regulatory cascade: JNK2 triggers NF-κB signaling activation to facilitate VSMC proliferation and migration, suppress contractile phenotype maintenance, and promote inflammatory secretion; miR-195-3p counteracts this pathological cascade by directly binding the 3'-UTR of JNK2 to repress JNK2 expression.

3.6 miR-195-3p exerts anti-atherosclerotic effects in high-fat diet-fed ApoE$^{-/-}$ mice

Based on the comprehensive in vitro cellular findings delineating miR-195-3p/JNK2/NF-κB regulatory axis, we further explored whether miR-195-3p confers atheroprotective effects in vivo. We delivered AAV-miR-195-3p or empty control AAV via tail vein injection into 6-week-old ApoE$^{-/-}$ mice, followed by 20 consecutive weeks of high-fat diet feeding (Fig. 6a). Oil Red O staining revealed significantly reduced atherosclerotic lesion burden in both the aortic root and the full-length aorta in AAV-miR-195-3p-treated mice (Fig. 6b, 6c). Hematoxylin-eosin (HE) staining and immunohistochemical staining against p-p65 further validated smaller plaque area and attenuated p65 phosphorylation within aortic lesions of miR-195-3p-overexpressing mice (Fig. 6d). Western blot analysis of total aortic tissue demonstrated reduced JNK2 and p-p65 protein levels, alongside elevated SMA and SM22α expression after AAV-miR-195-3p administration (Fig. 6e). ELISA quantification of circulating blood cytokines showed significantly

decreased concentrations of pro-inflammatory mediators IL-6, IL-8, TNF-α in the AAV-miR-195-3p group (Fig. 6f), which recapitulated our in vitro rescue assay observations.

Taken together, these in vivo data further corroborate our in vitro regulatory model: miR-195-3p exerts potent anti-atherosclerotic effects by negatively modulating JNK2 to restrain NF-κB cascade activation, thereby inhibiting pathological VSMC proliferation, migration and inflammatory reaction while preserving the contractile phenotype of vascular smooth muscle cells.

4. Discussion

Atherosclerosis stands as the dominant pathological substrate of life-threatening atherosclerotic cardiovascular diseases (ASCVD), including myocardial infarction, ischemic stroke and peripheral arterial disease, and remains the leading single cause of global mortality, responsible for over 10 million annual deaths worldwide with rapidly rising disease prevalence in low- and middle-income nations driven by aging and metabolic risk factor accumulation [18]. Current consensus frames atherosclerosis as a chronic, self-amplifying inflammatory disorder of the arterial wall, in which vascular smooth muscle cells (VSMCs)—the principal cellular constituent of the arterial media—act as central orchestrators of pathological vascular remodeling rather than passive bystanders of lipid deposition [19].Under homeostatic conditions, mature VSMCs maintain a quiescent contractile phenotype marked by high expression of α-SMA and SM22α to sustain vascular tension and structural integrity. However, persistent inflammatory cues within atherosclerotic microenvironments (encompassing TNF-α, IL-6, oxidized low-density lipoprotein and PDGF-BB) trigger VSMC dedifferentiation toward a synthetic state, characterized by robust proliferation, enhanced migratory capacity, excessive extracellular matrix secretion, and de novo synthesis of abundant pro-inflammatory mediators such as IL-6, IL-8 and TNF-α. A bidirectional vicious cycle links VSMC dysfunction and vascular inflammation: synthetic VSMCs secrete chemokines and cytokines to recruit circulating monocytes and amplify local inflammatory cascades, while accumulated immune-derived inflammatory signals further lock VSMCs in a pathological synthetic phenotype, jointly fueling neointimal hyperplasia, necrotic core expansion and fibrous cap thinning that precipitate plaque rupture and acute cardiovascular events [20]. Lineage-tracing studies further corroborate that transdifferentiated VSMCs contribute up to half of foam cell populations within human atherosclerotic lesions, reinforcing the inseparable interplay between VSMC phenotypic plasticity and inflammatory plaque evolution [21]. Against this well-established pathological backdrop, the present study systematically delineates a complete miR-195-3p/JNK2/NF-κB regulatory axis governing VSMC homeostasis via integrated evidence from clinical CAD plasma specimens, atherosclerotic ApoE$^{-/-}$ mouse aortas, multiple pathological VSMC in vitro models, and in vivo AAV-mediated miRNA overexpression assays. We verified that miR-195-3p is significantly downregulated under atherosclerotic pathological stimuli; restoration of miR-195-3p directly targets the 3'-UTR of JNK2 to suppress downstream canonical NF-κB inflammatory signaling, thereby reversing VSMC synthetic transformation, inhibiting aberrant proliferation and migration, and blunting pro-inflammatory cytokine secretion, ultimately mitigating aortic atherosclerotic lesion burden in hyperlipidemic mice. Collectively, this work

identifies an unreported miRNA-centered signaling cascade that bridges VSMC phenotypic regulation and vascular inflammation, expands the molecular regulatory network underlying atherosclerotic pathogenesis, and provides a candidate molecular target for anti-atherosclerotic intervention.

MicroRNAs (miRNAs) are short endogenous noncoding RNAs that suppress gene expression post-transcriptionally by binding the 3'-UTR of target mRNAs, acting as critical epigenetic regulators of vascular homeostasis [22]. A large body of evidence has validated multiple canonical miRNAs as core modulators of atherosclerosis through controlling endothelial function, macrophage lipid handling and VSMC phenotypic plasticity [23]. Representative molecules such as miR-143/145 preserve the contractile phenotype of VSMCs, while miR-21 and miR-221 drive pathological proliferation, migration and inflammation upon pro-atherogenic stimulation [24, 25]. The miR-195 subfamily belongs to the conserved miR-15/107 cluster and has attracted sustained research attention for its broad cardiovascular protective bioactivities. Existing investigations centered on miR-195 predominantly focus on its 5p arm (miR-195-5p). Early work in *Cardiovascular Research* reported that miR-195-5p restrains VSMC hyperplasia and neointimal thickening by targeting cell cycle genes [6]. Follow-up work further revealed that miR-195 represses M1 macrophage polarization and weakens paracrine crosstalk between macrophages and VSMCs, while clinical cohort evidence identified decreased circulating miR-195 as a potential diagnostic marker for aortic aneurysmal disease [5, 26]. In sharp contrast, functional investigations specific to miR-195-3p remain extremely scarce. Only one prior report uncovered its anti-atherosclerotic property in high methionine diet mice, which acts by targeting IL-31 to restrain macrophage inflammation; nevertheless, this study exclusively characterized myeloid cells and did not explore any direct regulatory effects of miR-195-3p on VSMC biological behaviors [4]. To date, no published studies have systematically clarified how miR-195-3p governs VSMC proliferation, phenotypic switching or inflammatory activation during atherogenesis, nor have any direct protein targets of miR-195-3p in VSMCs been validated. The present study addresses this critical unmet research demand by systematically dissecting the expression pattern, biological functions and downstream effector JNK2 of miR-195-3p in VSMCs.

Genetic knockout and pharmacological evidence have firmly established JNK2 as a master pro-atherogenic kinase, yet most existing studies dissect its pathogenic effects separately in macrophages and endothelial cells, with limited work systematically characterizing cell-autonomous JNK2 signaling that simultaneously drives VSMC phenotypic switching and downstream NF-κB-mediated inflammation [7, 27, 28]. Multiple lineage-tracing studies and in vitro assays confirmed that pathological stimuli such as ox-LDL and PDGF-BB trigger sustained JNK2 activation to boost VSMC proliferation and migration, two core events driving neointimal expansion [29]. A well-documented functional crosstalk exists between JNK2 and NF-κB signaling, the master transcriptional cascade controlling vascular inflammatory mediator release [27]. Published pharmacological and gene silencing experiments have confirmed that JNK2 promotes p65 phosphorylation and nuclear translocation to upregulate IL-6, IL-8 and TNF-α, whereas pan-JNK inhibition blunts NF-κB-mediated inflammation in VSMCs [13]. However, few prior reports integrate these VSMC phenotypic abnormalities with the NF-κB inflammatory transcriptional

cascade within a unified mechanistic framework. Our bioinformatic GSEA analysis of public atherosclerotic datasets further reinforced this linkage: JNK2-high aortic samples exhibited significant enrichment of TLR/NOD innate immune signaling, NF-κB cytokine production, and disrupted VSMC contractile structural pathways. The enrichment of lysosome pathway and tertiary granules further supports the role of the JNK2/NF-κB axis in promoting foam cell formation (via impaired lipid degradation) and neutrophil degranulation (via release of pro-inflammatory mediators), two critical events in plaque initiation and progression [30]. Moreover, the enrichment of contractile muscle fiber-related GOCC terms links JNK2-NF-κB activation to VSMC phenotypic switching, a process that drives vascular remodeling and plaque instability in advanced atherosclerosis [31]. Together, these data establish a mechanistic framework wherein JNK2 acts as a key regulator of the TLR/NF-κB inflammatory axis, coordinating both immune cell activation and vascular structural dysfunction to promote atherosclerotic pathogenesis. Our rescue assays with JNK2 overexpression, JNK inhibitor SP600125, and NF-κB agonist Diprovocim further clarified a layered regulatory hierarchy: miR-195-3p functions upstream to suppress JNK2, and JNK2 drives VSMC dysfunction through NF-κB activation. This layered model refines the linear JNK2-NF-κB pathway reported in previous single-target studies, offering a more comprehensive understanding of VSMC regulatory networks.

In vivo therapeutic delivery of microRNAs via adeno-associated virus (AAV) has become a mature preclinical strategy for atherosclerotic intervention in HFD-fed ApoE$^{-/-}$ mice, with multiple analogous miRNA overexpression models confirming stable vascular gene modulation and low systemic toxicity [32]. Our AAV-mediated in vivo intervention fully validated the robust anti-atherosclerotic capacity of miR-195-3p via direct repression of the JNK2/NF-κB cascade to restore VSMC homeostasis. Systemic overexpression of miR-195-3p in HFD-fed ApoE$^{-/-}$ mice successfully alleviated aortic lipid deposition, suppressed vascular inflammatory activation, and rescued the loss of contractile VSMC markers, which provides solid in vivo proof supporting the miR-195-3p/JNK2/NF-κB regulatory axis identified in cellular experiments. Nevertheless, we cannot exclude the possibility that miR-195-3p exerts additional atheroprotective effects through independent molecular pathways beyond JNK2 inhibition and NF-κB cascade. Existing transcriptomic and functional studies of the miR-195 subfamily have uncovered multiple downstream targets covering macrophage inflammatory signaling, endothelial oxidative injury and lipid metabolic programs, which indicates that miR-195-3p may simultaneously coordinate multi-cell-type protective networks within the arterial wall to restrain plaque progression [4, 5].

Beyond its mechanistic value for atherosclerosis pathogenesis, miR-195-3p also represents a promising candidate for miRNA-based cardiovascular therapeutics, aided by rapid advances in novel biomaterial delivery systems. Naked miRNA oligonucleotides suffer from rapid nuclease degradation and non-specific systemic clearance, restricting their clinical translation; viral vectors and non-viral nanocarriers including ionizable lipid nanoparticles, polymer micelles and stent-coating hydrogels have been widely optimized to enhance miRNA stability, vascular tissue targeting and cell-specific uptake [33, 34]. These innovative delivery platforms expand the clinical application scope of VSMC-regulatory miRNAs, especially for vascular disorders driven by excessive VSMC proliferation and synthetic transformation.

For instance, local miRNA-eluting stents and pulmonary-targeted lipid nanocarriers have demonstrated remarkable efficacy in preclinical models of in-stent restenosis and pulmonary arterial hypertension, two typical diseases characterized by pathological VSMC remodeling as the core pathological driver [35, 36]. Compared with traditional small-molecule vasoactive drugs that induce broad off-target suppression of cell proliferation, miRNA therapeutics can precisely tune VSMC phenotype at the post-transcriptional level without impairing physiological endothelial repair function, conferring broad translational prospects on miR-195-3p combined with vascular-targeted biomaterials for treating multiple proliferative vascular diseases beyond atherosclerosis [37].

Several limitations of this study should be acknowledged to guide future investigation. First, our clinical sampling only measured circulating miR-195-3p expression in CAD patient plasma, without collecting paired aortic vascular tissue specimens to detect local miR-195-3p and JNK2 expression within human atherosclerotic plaques. Second, constrained by research resources, we adopted systemic AAV2/9 injection to overexpress miR-195-3p in mice. Despite the inherent cardiovascular tropism of AAV2/9, this systemic delivery approach cannot restrict miR-195-3p overexpression exclusively to VSMCs, which may introduce confounding effects originating from endothelial cells and macrophages [38]. More sophisticated cell-specific strategies such as VSMC-targeted viral vectors or Cre-dependent CRISPR-Cas9 gene editing systems will help precisely characterize the cell-autonomous roles of miR-195-3p within vascular smooth muscle cells [39].Third, this work confirms NF-κB as one critical downstream effector of JNK2 in VSMC remodeling, yet additional JNK2-mediated signaling axes (e.g., AP-1) that contribute to VSMC dysfunction were not fully characterized in this study [40].

In summary, our work establishes miR-195-3p as an atheroprotective microRNA that restrains VSMC dysfunction and vascular inflammation through direct inhibition of JNK2 and suppression of NF-κB signaling. The newly uncovered miR-195-3p/JNK2/NF-κB pathway deepens our mechanistic understanding of vascular smooth muscle-dependent plaque development. Furthermore, this study lays a preclinical foundation for future translational research exploiting miRNA delivery systems to treat VSMC-driven vascular proliferative diseases.

Declarations

Acknowledgements

Not applicable.

Funding

This study was supported by the Postdoctoral Research Start-up Fund of the General Hospital of Central Theater Command (Grant No. BSH038).

Availability of data and materials

The sequencing data generated in the present study were deposited in the NCBI Sequence Read Archive (SRA) under the accession number PRJNA1537549 or at the following URL: https://www.ncbi.nlm.nih.gov/sra/PRJNA1537549. All the data generated in the present study may be requested from the corresponding author.

Authors' contributions

Pan Hou and Tongwei Lv performed the experiments, analyzed the data, and drafted the manuscript. Qing Lu reviewed the experimental data and revised the manuscript. Xianxian Zhao and Shifang Ding conceived the study design, interpreted the results, and responded to the reviewers' queries.

Ethics declarations

Human peripheral blood collection was conducted according to the guidelines of the Declaration of Helsinki and approved by the Ethics Committee of Shanghai Changhai Hospital (approval number: CHEC2024-212). Written informed consent was obtained from each participant or their next of kin.

All animal experiments were approved by the Animal Ethics Committee of Shanghai Changhai Hospital (approval number: CHEC (AE) 2023-001). Animal experiments were performed in compliance with the ARRIVE guidelines, institutional policies and national laboratory animal care and use regulations. Mice were housed under standard laboratory conditions with free access to food and water. All efforts were made to minimize animal suffering.

Patient consent for publication

Not applicable.

Conflicts of interest

The authors declare that they have no conflicts of interest.

References

1. Virani, S. S. et al. Heart Disease and Stroke Statistics-2021 Update: A Report From the American Heart Association. *Circulation* **143**, e254–e743 (2021).
2. Bennett, M. R., Sinha, S. & Owens, G. K. Vascular Smooth Muscle Cells in Atherosclerosis. *Circ. Res.* **118**, 692–702 (2016).
3. Bartel, D. P. Metazoan MicroRNAs. *Cell* **173**, 20–51 (2018).
4. Xiong, J. et al. miR-195-3p alleviates homocysteine-mediated atherosclerosis by targeting IL-31 through its epigenetics modifications. *Aging Cell.* **20**, e13485 (2021).
5. Bras, J. P. et al. miR-195 inhibits macrophages pro-inflammatory profile and impacts the crosstalk with smooth muscle cells. *Plos One*. **12**, e188530 (2017).

6. Wang, Y. S. et al. MicroRNA-195 regulates vascular smooth muscle cell phenotype and prevents neointimal formation. *Cardiovasc. Res.* **95**, 517–526 (2012).
7. Ricci, R. et al. Requirement of JNK2 for scavenger receptor A-mediated foam cell formation in atherogenesis. *Science* **306**, 1558–1561 (2004).
8. Oh, J. et al. Deletion of JNK2 prevents vitamin-D-deficiency-induced hypertension and atherosclerosis in mice. *J. Steroid Biochem. Mol. Biol.* **177**, 179–186 (2018).
9. Osto, E. et al. c-Jun N-terminal kinase 2 deficiency protects against hypercholesterolemia-induced endothelial dysfunction and oxidative stress. *Circulation* **118**, 2073–2080 (2008).
10. Zhan, Y. et al. Role of JNK, p38, and ERK in platelet-derived growth factor-induced vascular proliferation, migration, and gene expression. *Arterioscler. Thromb. Vasc Biol.* **23**, 795–801 (2003).
11. Xin, Y. et al. Elucidating VSMC phenotypic transition mechanisms to bridge insights into cardiovascular disease implications. *Front. Cardiovasc. Med.* **11**, 1400780 (2024).
12. Chen, X. et al. JNK Pathway-Associated Phosphatase Deficiency Facilitates Atherosclerotic Progression by Inducing T-Helper 1 and 17 Polarization and Inflammation in an ERK- and NF-κB Pathway-Dependent Manner. *J. Atheroscler Thromb.* **31**, 1460–1478 (2024).
13. Chen, Y. Y. et al. Andrographolide inhibits nuclear factor-κB activation through JNK-Akt-p65 signaling cascade in tumor necrosis factor-α-stimulated vascular smooth muscle cells. *ScientificWorldJournal* **2014**, 130381 (2014).
14. Hayakawa, E. et al. Overexpression of receptor for advanced glycation end products induces monocyte chemoattractant protein-1 expression in rat vascular smooth muscle cell line. *J. Atheroscler Thromb.* **19**, 13–22 (2012).
15. Battes, L. C. et al. Circulating cytokines in relation to the extent and composition of coronary atherosclerosis: results from the ATHEROREMO-IVUS study. *Atherosclerosis* **236**, 18–24 (2014).
16. Bennett, B. L. et al. SP600125, an anthrapyrazolone inhibitor of Jun N-terminal kinase. *Proc. Natl. Acad. Sci. U S A*. **98**, 13681–13686 (2001).
17. Chen, C. C. et al. Corylin Inhibits Vascular Cell Inflammation, Proliferation and Migration and Reduces Atherosclerosis in ApoE-Deficient Mice. *Antioxidants (Basel)* 9. (2020).
18. Zaman, S. et al. The Lancet Commission on rethinking coronary artery disease: moving from ischaemia to atheroma. *Lancet* **405**, 1264–1312 (2025).
19. Chen, R. et al. Phenotypic Switching of Vascular Smooth Muscle Cells in Atherosclerosis. *J. Am. Heart Assoc.* **12**, e31121 (2023).
20. Yurdagul, A. J. Crosstalk Between Macrophages and Vascular Smooth Muscle Cells in Atherosclerotic Plaque Stability. *Arterioscler. Thromb. Vasc Biol.* **42**, 372–380 (2022).
21. Wang, Y. et al. Smooth Muscle Cells Contribute the Majority of Foam Cells in ApoE (Apolipoprotein E)-Deficient Mouse Atherosclerosis. *Arterioscler. Thromb. Vasc Biol.* **39**, 876–887 (2019).
22. Ciavarella, C. et al. Heterogeneity and Differentiation of the Human Arterial Tree: Focus on microRNA Expression in Vascular Disease. *Biomolecules* 14. (2024).

23. Lu, Y. et al. Impact of miRNA in Atherosclerosis. *Arterioscler. Thromb. Vasc Biol.* **38**, e159–e170 (2018).
24. Cordes, K. R. et al. miR-145 and miR-143 regulate smooth muscle cell fate and plasticity. *Nature* **460**, 705–710 (2009).
25. Kang, H. & Hata, A. MicroRNA regulation of smooth muscle gene expression and phenotype. *Curr. Opin. Hematol.* **19**, 224–231 (2012).
26. Zampetaki, A. et al. Role of miR-195 in aortic aneurysmal disease. *Circ. Res.* **115**, 857–866 (2014).
27. Pan, H. et al. Anti-JNK2 peptide-siRNA nanostructures improve plaque endothelium and reduce thrombotic risk in atherosclerotic mice. *Int. J. Nanomed.* **13**, 5187–5205 (2018).
28. Sumara, G., Belwal, M. & Ricci, R. Jnking atherosclerosis. *Cell. Mol. Life Sci.* **62**, 2487–2494 (2005).
29. Chang, Y. et al. Platonin inhibited PDGF-BB-induced proliferation of rat vascular smooth muscle cells via JNK1/2-dependent signaling. *Acta Pharmacol. Sin*. **32**, 1337–1344 (2011).
30. Gui, Y., Zheng, H. & Cao, R. Y. Foam Cells in Atherosclerosis: Novel Insights Into Its Origins, Consequences, and Molecular Mechanisms. *Front. Cardiovasc. Med.* **9**, 845942 (2022).
31. Yu, Y. et al. Vascular smooth muscle cell phenotypic switching in atherosclerosis. *Heliyon* **10**, e37727 (2024).
32. Lu, X. et al. MicroRNA-320b Modulates Cholesterol Efflux and Atherosclerosis. *J. Atheroscler Thromb.* **29**, 200–220 (2022).
33. Saenz-Pipaon, G. & Dichek, D. A. Targeting and delivery of microRNA-targeting antisense oligonucleotides in cardiovascular diseases. *Atherosclerosis* **374**, 44–54 (2023).
34. He, S. & Li, X. Bridging miRNA Research with Clinical Applications in Cardiovascular Diseases: Advances in Delivery Systems and Therapeutic Strategies. *Mini Rev. Med. Chem.* **26**, 144–161 (2026).
35. McLendon, J. M. et al. Lipid nanoparticle delivery of a microRNA-145 inhibitor improves experimental pulmonary hypertension. *J. Control Release*. **210**, 67–75 (2015).
36. Wang, D. et al. Local MicroRNA Modulation Using a Novel Anti-miR-21-Eluting Stent Effectively Prevents Experimental In-Stent Restenosis. *Arterioscler. Thromb. Vasc Biol.* **35**, 1945–1953 (2015).
37. Santulli, G. et al. A selective microRNA-based strategy inhibits restenosis while preserving endothelial function. *J. Clin. Invest.* **124**, 4102–4114 (2014).
38. Chen, Q. et al. Recombinant adeno-associated virus serotype 9 in a mouse model of atherosclerosis: Determination of the optimal expression time in vivo. *Mol. Med. Rep.* **15**, 2090–2096 (2017).
39. Deaton, R. A. et al. A New Autosomal Myh11-CreER(T2) Smooth Muscle Cell Lineage Tracing and Gene Knockout Mouse Model-Brief Report. *Arterioscler. Thromb. Vasc Biol.* **43**, 203–211 (2023).
40. Yoshizumi, M. et al. Quercetin glucuronide prevents VSMC hypertrophy by angiotensin II via the inhibition of JNK and AP-1 signaling pathway. *Biochem. Biophys. Res. Commun.* **293**, 1458–1465 (2002).

Figures

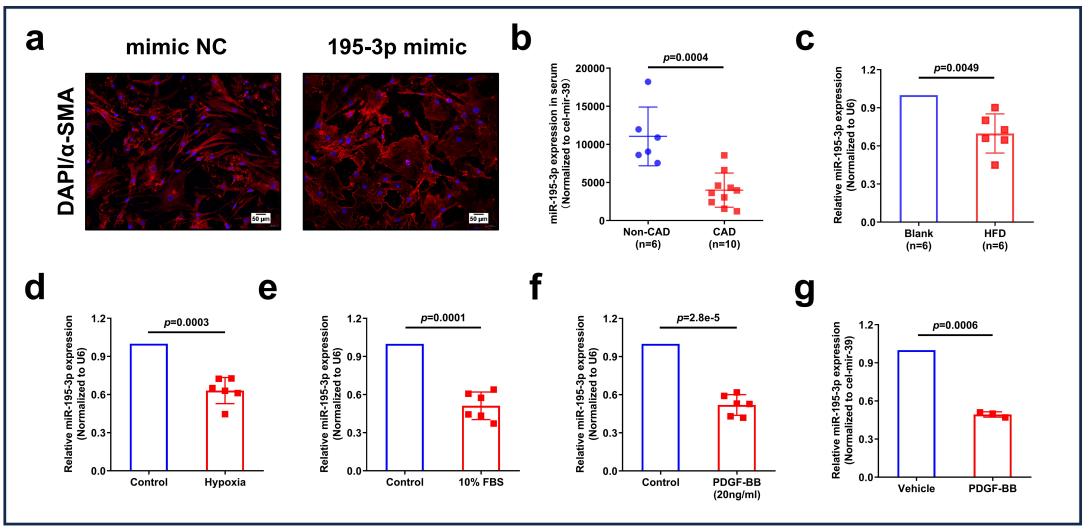


Figure 1

miR-195-3p is downregulated in patients with coronary artery disease, atherosclerotic animal models, and vascular smooth muscle cells exposed to diverse pathological stimuli. (a) Representative immunofluorescence images of alpha-smooth muscle actin (α-SMA) in vascular smooth muscle cells

(VSMCs) transfected with miR-195-3p mimic or mimic negative control (mimic NC). Blue indicates nuclei stained with DAPI, and red indicates α-SMA. Scale bar =50μm. **(b)** Scatter plot of relative miR-195-3p expression in serum from patients in the non-coronary artery disease (non-CAD) and the coronary artery disease (CAD,). **(c)** Relative expression of miR-195-3p in serum from mice in the blank control group (Blank,) and the high-fat diet group (HFD). **(d)** Relative miR-195-3p expression in VSMCs from the normoxia control group (Control) and the hypoxia treatment group (Hypoxia). **(e)** Relative miR-195-3p expression in VSMCs from the control group (Control) and the 10% fetal bovine serum stimulation group (10%FBS). **(f)** Relative miR-195-3p expression in VSMCs from the control group (Control) and the platelet-derived growth factor-BB stimulation group (PDGF-BB, 20 ng/ml). **(g)** Relative miR-195-3p expression in exosomes secreted by VSMCs from the vehicle control group (Vehicle) and the PDGF-BB stimulation group (PDGF-BB). Data were presented as mean ± SD (scatter dots in scatter plots and bar charts represent independent biological replicates). The P value was determined by unpaired t-test for data with equal variance(b) or Welch's t test when variances were unequal (c through g), with the significance threshold set at $\alpha = 0.05$.

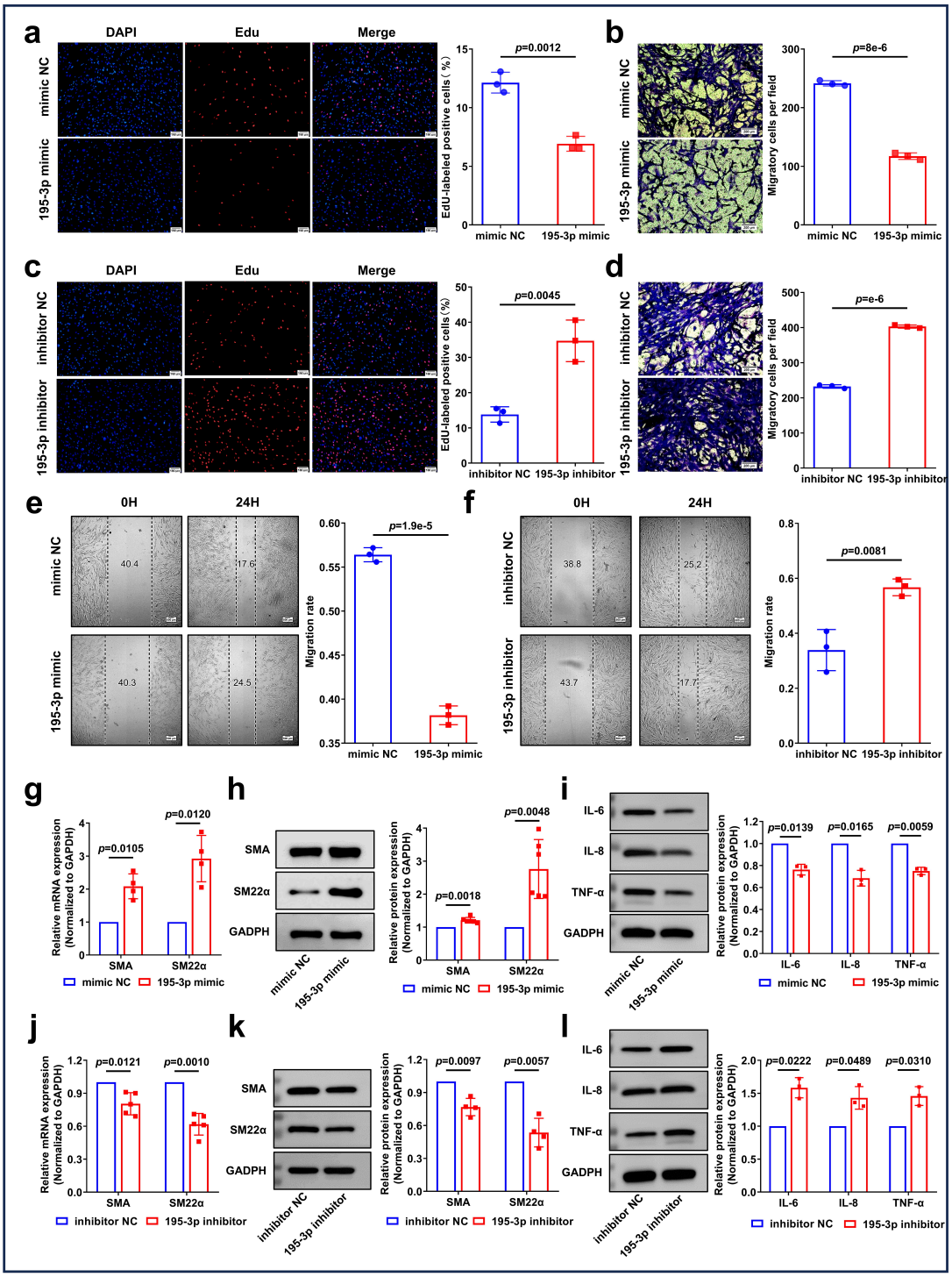


Figure 2

miR-195-3p regulates the proliferation, migration, contractile phenotype, and inflammatory response of vascular smooth muscle cells. (a, c) Cell proliferation was assessed using the 5-ethynyl-2'-deoxyuridine (EdU) incorporation assay after transfection with miR-195-3p mimic or inhibitor. Scale bar =100μm. **(b, d)** Transwell chamber assays were performed to evaluate the migration and invasion abilities of VSMCs after transfection with miR-195-3p mimic or inhibitor. Scale bar =200μm. **(e, f)** Two-

dimensional cell migration was assessed using the wound healing assay after transfection with miR-195-3p mimic or inhibitor. Scale bar =500μm. **(g, j)** The mRNA expression levels of the contractile phenotype markers alpha-smooth muscle actin (α-SMA) and smooth muscle 22 alpha (SM22-α) were measured by real-time quantitative PCR (RT-qPCR) after transfection with miR-195-3p mimic or inhibitor. **(h, k)** The protein expression levels of α-SMA and SM22-α were detected by Western blot after transfection with miR-195-3p mimic or inhibitor. **(i, l)** The protein expression levels of the inflammatory cytokines interleukin-6 (IL-6), interleukin-8 (IL-8), and tumor necrosis factor-α (TNF-α) were detected by Western blot after transfection with miR-195-3p mimic or inhibitor. Data were presented as mean ± SD (scatter dots in scatter plots and bar charts represent independent biological replicates). The P value was determined by unpaired t-test for data with equal variance (a through f) or Welch's t test when variances were unequal (g through l), with the significance threshold set at $\alpha = 0.05$.

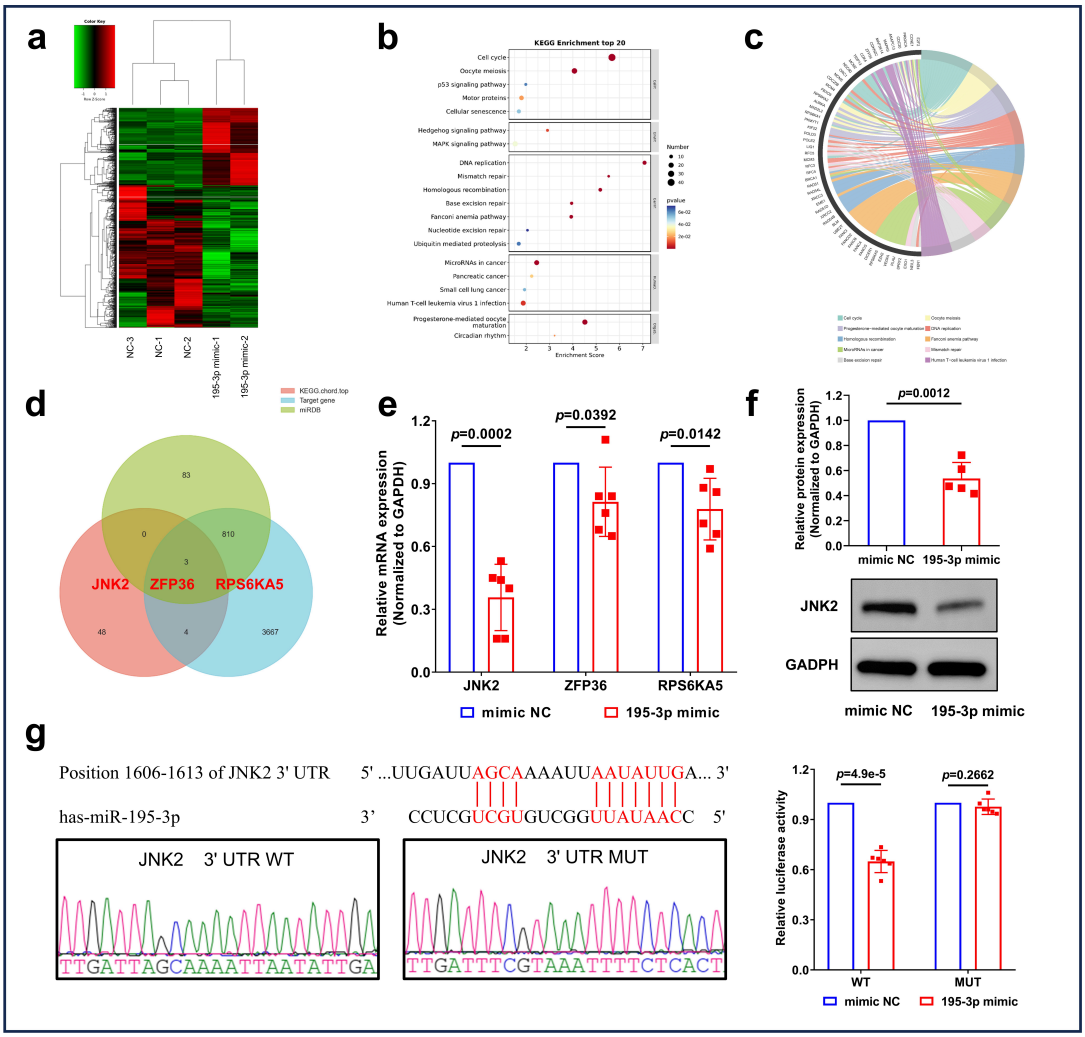


Figure 3

miR-195-3p directly binds to the 3' UTR of JNK2 and represses its expression. (a) Clustered heatmap showing differentially expressed genes obtained from RNA sequencing following miR-195 3p overexpression. Gene expression patterns are compared between the control (mimic NC) and miR-195 3p overexpressing groups (195-3p mimic). Red indicates high gene expression, and blue indicates low gene expression. (b) Bubble plot for Kyoto Encyclopedia of Genes and Genomes (KEGG) pathway

enrichment analysis of down-regulated gens. (c) Chord diagram visualizing the association network between KEGG enriched top genes and pathways. (d) Venn diagram illustrating overlapping candidate target gene screening results. Candidate targets JNK2 (c Jun N terminal kinase 2), RPS6KA5(Mitogen- and stress-activated protein kinase 1) and ZFP36 (Zinc finger protein 36) were identified by intersecting KEGG enriched top genes with genes predicted by TargetScan and miRDB databases. (e) mRNA expression of candidate target genes in VSMCs transfected with miR-195-3p mimic measured by RT qPCR. (f) Protein abundance of JNK2 in VSMCs transfected with miR-195-3p mimic detected by Western blot. (g) Dual luciferase reporter assay validating direct targeting of JNK2 by miR-195 3p. Left panel: sequence alignment and sequencing chromatograms of wild type (JNK2 3' UTR WT, containing the predicted binding site) and mutant (JNK2 3' UTR MUT) reporter constructs. Right panel: miR-195 3p mimic substantially repressed luciferase activity of the WT reporter relative to mimic NC. Data were presented as mean ± SD (scatter dots in scatter plots and bar charts represent independent biological replicates). The P value was determined by Welch’s t test because variances were unequal (e through f), with the significance threshold set at $\alpha = 0.05$.

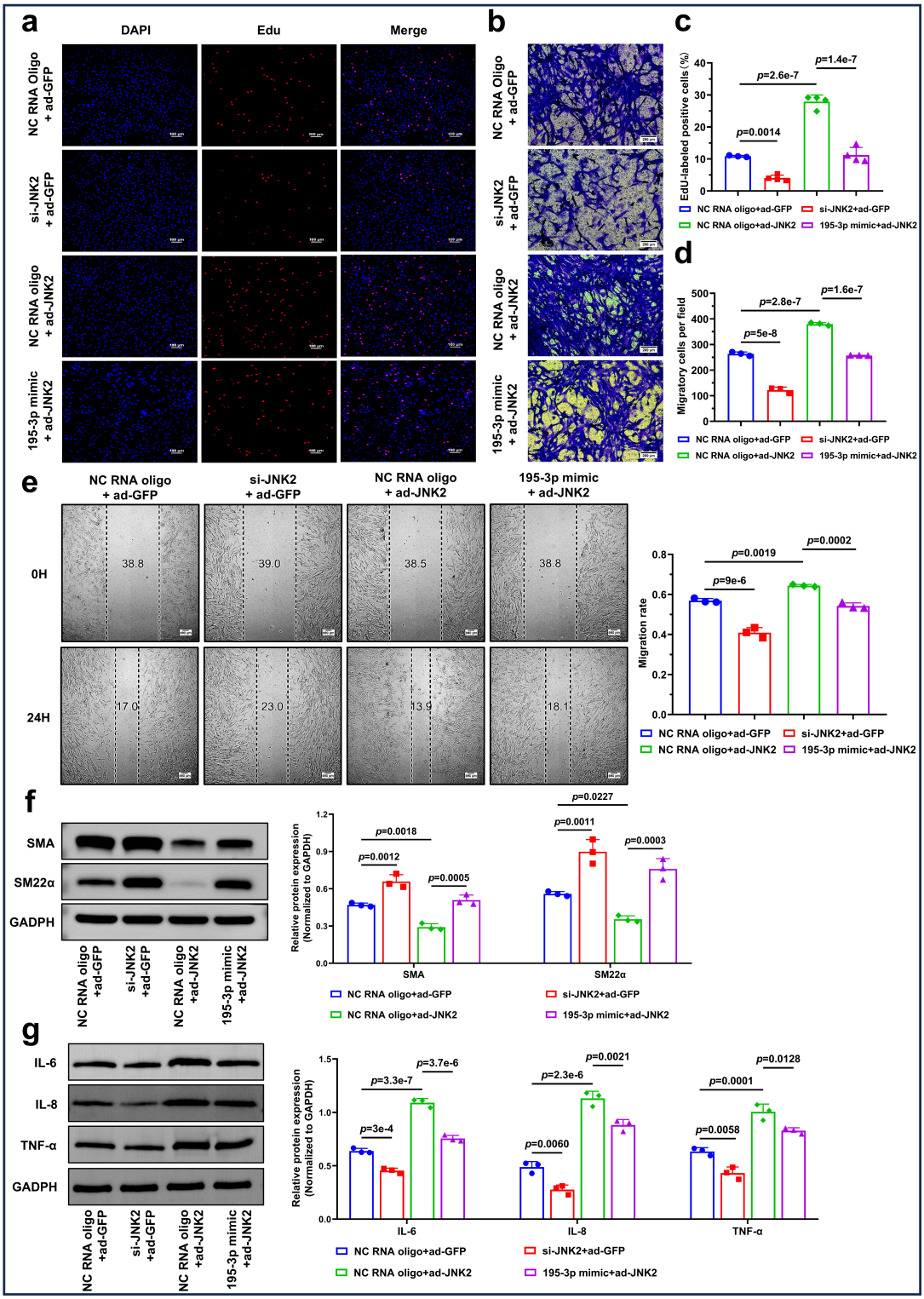


Figure 4

miR-195-3p regulates JNK2-driven proliferation, migration, phenotypic switching and inflammatory response of vascular smooth muscle cells. (a, c) EdU incorporation assay for evaluation of proliferative capacity in vascular smooth muscle cells (VSMCs). (a) Representative immunofluorescence images; cell nuclei were counter-stained with DAPI (blue), and proliferating cells were labelled by EdU (red). Scale bar =100μm. (c) Quantification of the percentage of EdU-positive cells. Four experimental groups were

included: control (NC RNA Oligo + ad-GFP), JNK2 knockdown (si-JNK2 + ad-GFP), JNK2 overexpression (NC RNA Oligo + ad-JNK2), and co-treatment with miR-195-3p mimic plus JNK2 overexpression (195-3p mimic + ad-JNK2). (b, d) Transwell chamber assay to assess migratory capacity of VSMCs. (b) Representative microscopic images. Scale bar =200μm. (d) Quantification of migrated cell number per field. Experimental groups were consistent with the Edu data. (e) Wound-healing assay assessing two-dimensional migratory capacity of VSMCs. Left panel: scratch-wound micrographs acquired at 0 h and 24 h; dashed lines delineate wound boundaries. Scale bar =600μm. Right panel: quantitative analysis of migration rates. Experimental groups were consistent with the Edu data. (f) Western blot analysis for contractile VSMC phenotype markers α-SMA and SM22-α. Left panel: representative immunoblot bands. Right panel: quantitative analysis of relative protein expression normalized to GAPDH. Experimental groups were consistent with the Edu data. (g) Western blot analysis for inflammatory cytokines interleukin-6 (IL-6), interleukin-8 (IL-8), and tumor necrosis factor-α (TNF-α). Left panel: representative immunoblot bands. Right panel: quantitative analysis of relative protein expression normalized to GAPDH. Experimental groups were consistent with the Edu data. Data were presented as mean ± SD (scatter dots in bar charts represent independent biological replicates). Multiple-group comparisons were performed using one-way ANOVA followed by Tukey's multiple-comparison test, with the significance threshold set at $\alpha = 0.05$.

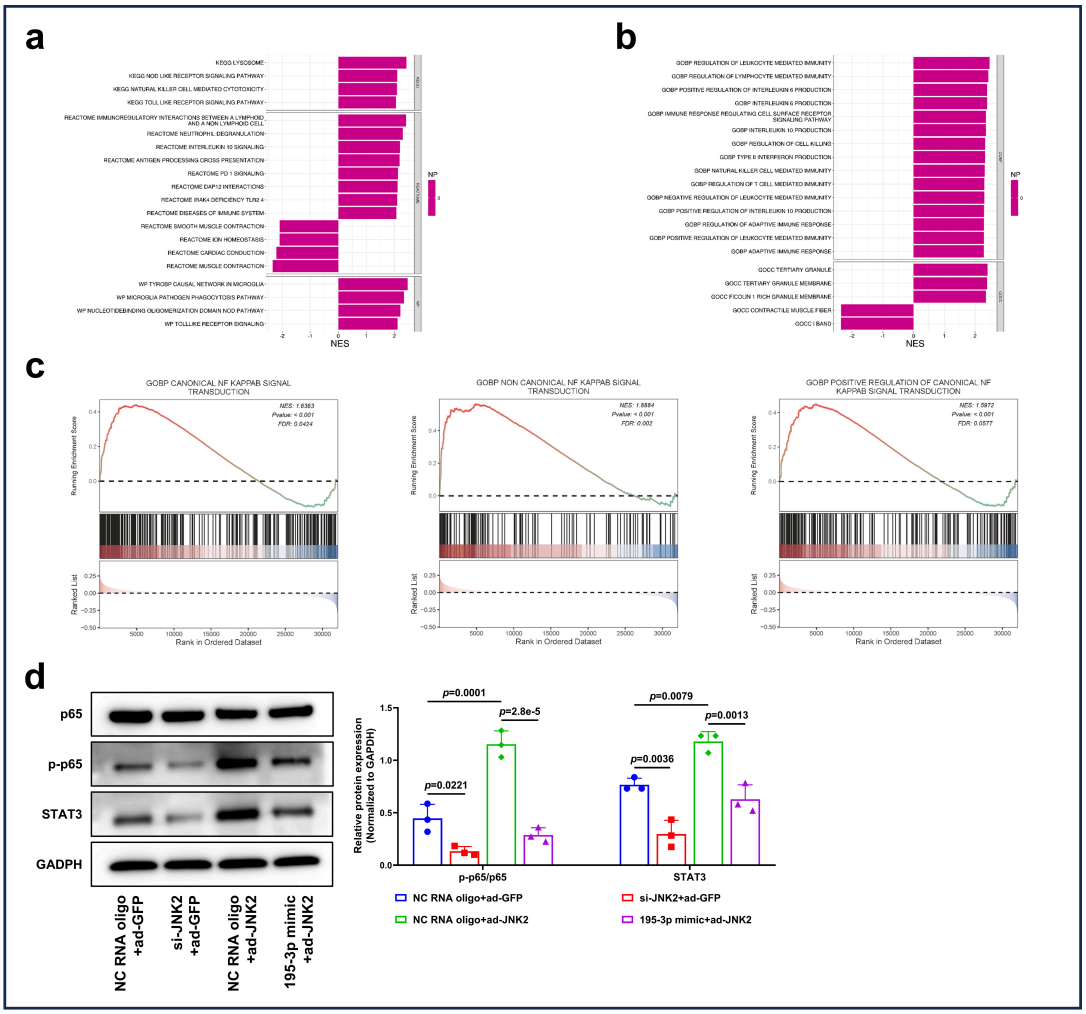


Figure 5

miR-195-3p/JNK2 axis exerts its function by modulating the NF-κB signaling pathway. (a) Plot of KEGG pathway-enrichment analysis. KEGG enrichment of differentially expressed genes derived from transcriptomic data of the JNK2-high-expression group. Screening thresholds were nominal p-value (NP) < 0.05 and false discovery rate (FDR) < 0.25.(b) Plot of Gene Ontology Biological Process (GOBP) enrichment analysis. Multiple biological processes satisfied the above-mentioned significance criteria,

such as leukocyte/lymphocyte-mediated immunity, positive regulation of IL-6 biosynthesis and adaptive immune responses (all NES > 2, P < 0.05). (c) Gene Set Enrichment Analysis (GSEA) enrichment plot visualizing enrichment of NF-κB-signaling-related pathways. (d) Western-blot detection of key proteins of the NF-κB signaling pathway, including phosphorylated p65 (p-p65), total p65, and signal transducer and activator of transcription 3 (STAT3). Four experimental groups were included: control (NC RNA Oligo + ad-GFP), JNK2 knockdown (si JNK2 + ad-GFP), JNK2 overexpression (NC RNA Oligo + ad JNK2), and co treatment with miR-195-3p mimic plus JNK2 overexpression (195-3p mimic + ad JNK2). Left panel: representative immunoblot bands. Right panel: quantitative analysis of relative protein expression normalized to GAPDH. Bioinformatic analyses in panels (a), (b), and (c) were performed with rigorous multiple-hypothesis-testing correction (nominal p-value < 0.05, FDR < 0.25). Data are presented as mean ± SD (scatter dots represent independent biological replicates). Multiple-group comparisons were performed using one-way ANOVA followed by Tukey's multiple-comparison test, with the significance threshold set at $\alpha = 0.05$.

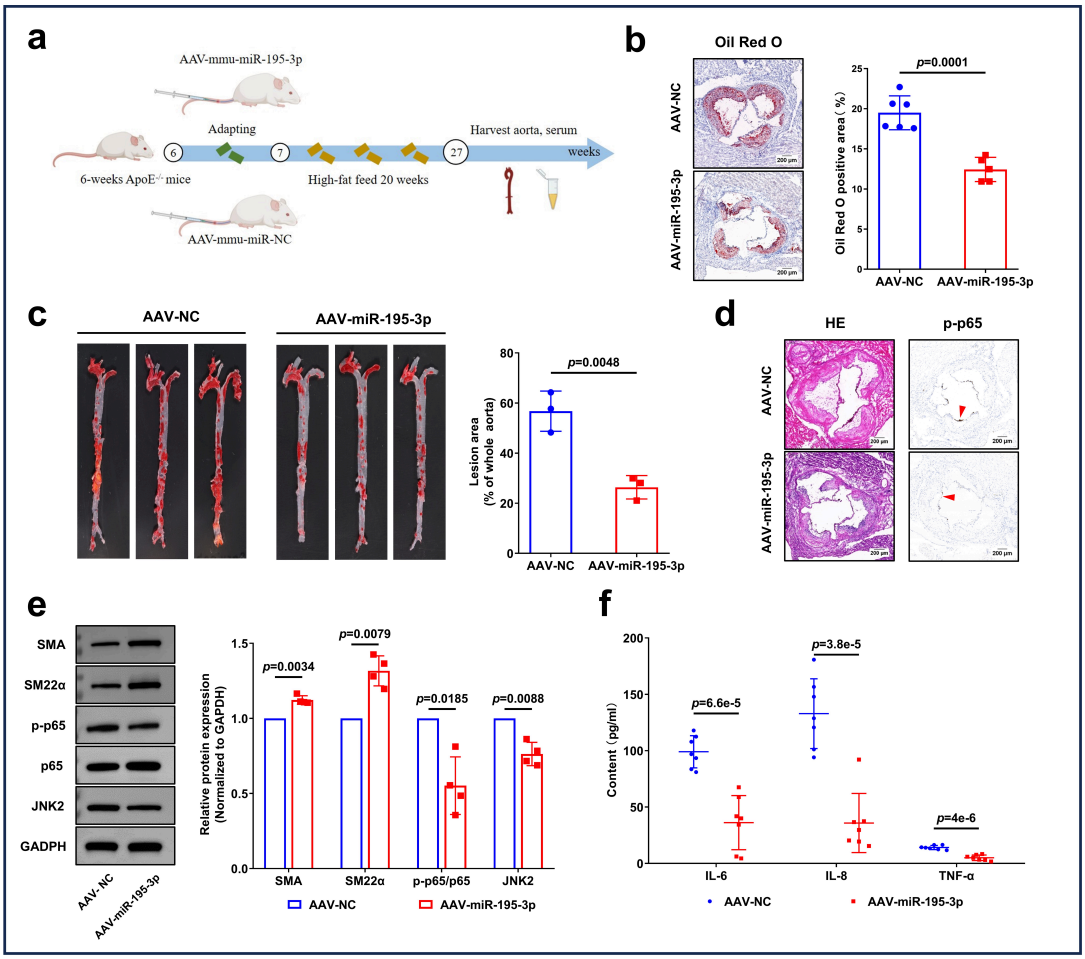


Figure 6

Overexpression of miR-195-3p in vivo attenuates atherosclerotic lesions and inhibits NF-κB-mediated vascular inflammation in ApoE mice. (a) Schematic illustration of the experimental design and timeline for the atherosclerotic mouse model. Six-week-old specific pathogen-free (SPF) male apolipoprotein E-deficient (ApoE) mice were acclimated for one week and randomly assigned to two groups: AAV-negative control group (AAV-NC) and miR-195-3p-overexpressing adeno-associated virus group (AAV-

miR-195-3p). All mice were fed a high-fat diet (HFD) for 20 weeks to induce atherosclerotic plaque formation. Serum and aortic tissues were collected at the experimental endpoint for subsequent analysis. (b) Representative Oil Red O staining images and quantitative analysis of lipid deposition area in the aortic root. Scale bar =200μm. (c) Representative en face Oil Red O staining images and statistical quantification of atherosclerotic lesion area in the entire aorta. (d) Representative hematoxylin-eosin (H&E) staining and p-p65 immunohistochemistry (IHC) staining of the aortic root. Scale bar =200μm. (e) Western blot analysis of VSMC contractile phenotype markers (α-SMA, SM22-α) and core NF-κB signaling proteins (p-p65, total p65, JNK2) in aortic tissues. Left panel: representative immunoblot bands. Right panel: quantitative analysis of relative protein expression normalized to GAPDH. (f) Enzyme-linked immunosorbent assay (ELISA) detection of serum inflammatory cytokines, including IL-6, IL-8 and TNF-α. Data are presented as mean ± SD, and scatter dots represent independent biological samples. The P value was determined by unpaired t test for data with equal variance (b, c, f) or Welch's t test when variances were unequal (e). The significance threshold was set at α = 0.05.

Supplementary Files

This is a list of supplementary files associated with this preprint. Click to download.

- SupplementalMaterial1.docx
- SupplementalMaterial2originalWesternblots.pdf
- FigureS1.jpg
- FigureS2.jpg